A New Multidimensional Spectral and Polarization Information Detection Technology

Yechao Wang, Xiaoli Chen, Xiaoming Zhong, and Haibo Zhao

Abstract Simultaneous acquisition of spectral information and polarized information can obtain more feature information to distinguish targets. Based on the computational imaging technology and a pixelized polarization detector, we propose a novel imaging mode that simultaneously acquires 2D spatial information, 1D spectral information and 1D spectral–polarized information of the target. In the framework of compressed sensing, the imaging results are obtained by the pixelized polarization detector after the spatial modulation of coded aperture and the dispersion of prism. The corresponding spectral and polarization images are reconstructed by an optimization algorithm. The method can obtain 25 bands of spectral and polarization images of four angles (0°, 45°, 90° and 135°), ranging in 450–650 nm (spectral resolution less than 10 nm), and the degree of linear polarization and the angle of polarization of each band. The experimental prototype has been developed, and the data acquisition and processing have been completed. Finally, the technology has successfully achieved simultaneous acquisition of multidimensional spatial–spectral–polarized information.

Keywords Computational imaging · Polarization detector · Multidimensional information · Spectral image reconstruction

1 Introduction

Traditional spectropolarimeter can simultaneously acquire three-dimensional spatial–spectral data of each Stokes parameter by scanning specific domains [1], such as the spatial domain in channeled spectropolarimetry [2], the optical path difference domain in Fourier transform imaging spectropolarimetry [3] and polarization domain in other spectropolarimetry [4]. Some new systems obtain polarization spectra by direct measurements such as integrating integral field spectrometry with division-of-aperture imaging polarimetry [5]. However, the above systems have limitations such

Y. Wang (✉) · X. Chen · X. Zhong · H. Zhao
Beijing Institute of Space Mechanics & Electricity, Beijing, China
e-mail: cast_wangyc_508@163.com

© Springer Nature Singapore Pte Ltd. 2020

L. Wang et al. (eds.), *Proceedings of the 6th China High Resolution Earth Observation Conference (CHREOC 2019)*, Lecture Notes in Electrical Engineering 657,
https://doi.org/10.1007/978-981-15-3947-3_1

as noise sensitivity, channel cross talk and spectral resolution [6, 7]. Some literatures have introduced the latest compressed spectral imaging method, using channel switching method to measure polarization spectrum, but at the expense of time resolution [8]. Compressed spectrum imaging is a new technology that has evolved in recent years. Based on the compressed sensing framework, high-dimensional snapshot acquisition of spectral information becomes possible [9]. The coded aperture snapshot spectral imager (CASSI) receives information from the array detector by random code modulation of the scene and spectral modulation of the dispersive elements [10–12]. Inspired by this, we propose a new imaging mode that a pixelized polarization detector combined with compression spectroscopy to simultaneously detect two-dimensional spatial information (x, y), one-dimensional spectral information (λ) and four polarized components (0°, 45°, 90° and 135°). The random coded aperture enables the system to code of the spatial information efficiently, and the integration of the polarization detector with the CASSI achieves efficient acquisition. The feasibility of the scheme was verified by experiments, and the model of the system was established. Under the theory of compressed sensing, the optimization problem is solved by the iterative algorithm. This model breaks through the principle limitation of the traditional polarization spectrum detection method and satisfies the synchronous acquisition requirements of multidimensional information such as time-space spectrum polarization.

The scene information $h(x, y, \lambda, p)$ is limited by bandpass filter (BPF), and then it is modulated by coded aperture (CA). After double Amici prism (DAP) dispersion modulation, it is imaged on the polarization detector.

2 A New Multidimensional Spectral and Polarization Information Detection Technology

The principle of the multidimensional polarization spectrum detection system is shown in Fig. 1. The scene information $h(x, y, \lambda, p)$ first enters the objective lens, and the bandpass filter of 450–650 nm is used to intercept the spectrum segments.

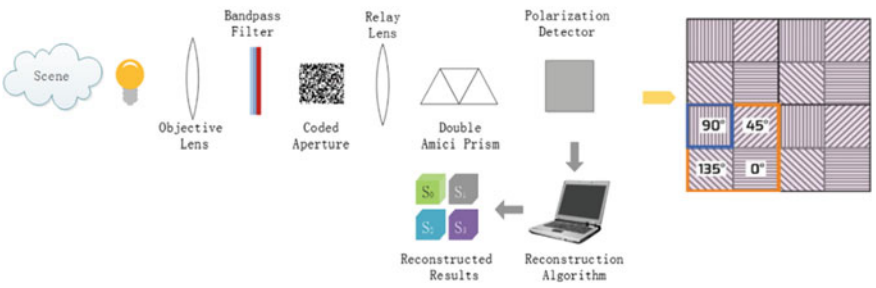

Fig. 1 Schematic of system

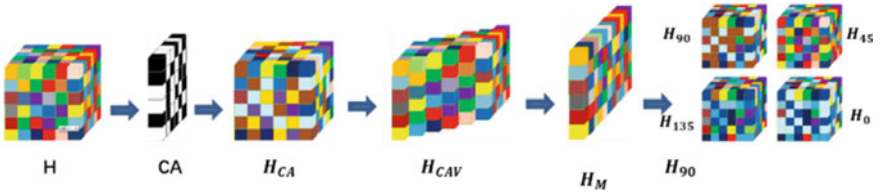

Fig. 2 Data modulation flowchart

Then, the light reaches the coded aperture, and the random coding mask spatially modulates the information $h(x, y, \lambda, p)$. The coded aperture is a random matrix and sets 0 and 1 channels which etched on the glass and made an anti-reflectance process. The light which is modulated by the codes goes through the relay lens and then reaches the dispersive element. Then, a double Amici prism is used to disperse the encoded light from the spectral dimension. It is useful for subsequent reconstruction of the data cube. The coded information passes through the dispersive prism and reaches the polarization detector. A spatially encoded and dispersion-modulated polarization spectrum-compressed image is obtained on the polarization detector (Fig. 2).

The data flowchart indicates that the information H first performs coding of 0 or 1 in space when it passes through the coded aperture (CA). After the dispersion of the double Amici prism, the data cube is expressed as H_{CAV} and it is distributed on both sides of the central wavelength of 550 nm. H_{M} is obtained on the polarization detector, including four polarization components (0°, 45°, 90°, and 135°).

3 System Model

As shown in Fig. 1, the scene information can be expressed as $h(x, y, \lambda, p)$, where x and y represent two-dimensional spatial information, λ represents spectral information, and $p = 0, 1, 2, 3$, representing different polarization information,

$$\boldsymbol{S}_{\mathbf{out}} = \boldsymbol{M}_{\mathbf{pd}} \boldsymbol{S}_{\mathbf{in}} \tag{1}$$

$$\boldsymbol{M}_{\mathbf{pd}}(\theta) = \frac{1}{2} \begin{bmatrix} 1 & \cos 2\theta & \sin 2\theta & 0 \\ \cos 2\theta & \cos^2 2\theta & \cos 2\theta \sin 2\theta & 0 \\ \sin 2\theta & \cos 2\theta \sin 2\theta & \sin^2 2\theta & 0 \\ 0 & 0 & 0 & 0 \end{bmatrix} \tag{2}$$

$$\mathbf{S} = \left[\boldsymbol{S}_0^{\mathrm{T}}, \boldsymbol{S}_1^{\mathrm{T}}, \boldsymbol{S}_2^{\mathrm{T}}, \boldsymbol{S}_3^{\mathrm{T}}\right]^{\mathbf{T}} \tag{3}$$

M_{pd} represents the Mueller matrix of the polarization detector [13]. $\boldsymbol{S}_{\mathbf{in}}$ and $\boldsymbol{S}_{\mathbf{out}}$ represent polarization information of incident and outgoing light. Due to the small field of the lens, the Mueller matrix of other components can be considered as a unit

matrix. S is Stokes parameter [14]. Similar to the CASSI, the image acquired by the detector can be expressed as [15]

$$f(x, y) = \sum_{p=0}^{3} \int \psi_{\mathrm{P}}(x, y, \lambda) T(x, y, \lambda) h(x, y, \lambda, p) \mathrm{d}\lambda + \omega(x, y) \tag{4}$$

$\psi_{\mathrm{P}}(x, y, \lambda)$ represents the modulation of the polarizer. $T(x, y, \lambda)$ is the modulation introduced by the CASSI, and $\omega(x, y)$ is system noise. Discrete form can be expressed as

$$f(m, n) = \sum_{p=0}^{3} \sum_{k=1}^{25} \psi_{\mathrm{P}}(m, n, \lambda) T(m, n, k) h(m, n, k, p) + \omega(x, y) \tag{5}$$

(m, n) is the discrete coordinate, and k is the number of spectral bands. Expressed as matrix forms,

$$\boldsymbol{F} = \boldsymbol{\Psi T H} + \boldsymbol{\Omega} = \boldsymbol{K H} + \boldsymbol{\Omega} \tag{6}$$

$\boldsymbol{F}$, $\boldsymbol{\Psi}$, $\mathbf{T}$, $\boldsymbol{H}$, $\boldsymbol{\Omega}$ are the matrix forms of $\psi_P(m, n, \lambda)$, $T(m, n, k)$, $h(m, n, k, p)$ and $\omega(x, y)$. $\mathbf{K} = \boldsymbol{\Psi}\mathbf{T}$ is the measurement matrix of the system. Assume that the data cube has L spectral bands, $M \times N$ spatial pixels and 4 Stokes parameters. It can be expressed as

$$\boldsymbol{F} = [\boldsymbol{K}_0, \boldsymbol{K}_1, \boldsymbol{K}_2, \boldsymbol{K}_3]\left[\boldsymbol{H}_{\mathbf{0}}^{\mathbf{T}}, \boldsymbol{H}_{\mathbf{1}}^{\mathbf{T}}, \boldsymbol{H}_{\mathbf{2}}^{\mathbf{T}}, \boldsymbol{H}_{\mathbf{3}}^{\mathbf{T}}\right] + \boldsymbol{\Omega} \tag{7}$$

K_{p} is the measurement matrix of $\boldsymbol{S}_{\mathbf{p}} \in \Re^{\boldsymbol{MNL}\times 1}$,and $\boldsymbol{F} \in \Re^{\boldsymbol{MN+L}-1\times 1}$ is the vectorized form of f.

4 Reconstruction Algorithm

The original polarization spectrum information is obtained by solving an optimization problem. We need to reconstruct all the original information from an incomplete observation. Due to the sparsity of the spectral data itself, the underdetermined system can find a unique solution by solving the following optimization problem [16],

$$\widehat{\boldsymbol{F}} = \arg\min_{\boldsymbol{F}} \left\| \boldsymbol{G} - \mathbf{H}\mathbf{F}_{\mathbf{2}}^{\mathbf{2}} \right\| + \tau \Gamma(\boldsymbol{F}) \tag{8}$$

where $\boldsymbol{G}$ is the observed value, $\boldsymbol{H}$ is the equivalent observation matrix, $\boldsymbol{F}$ is the scene spectral data, and τ is a parameter used to adjust the balance between the two parts.

Formula (8) is the objective function of the optimization and consists of two parts: (a) the system fidelity term, which is used to measure the error between the

optimization result and the system observation, and (b) the regularization term, which is generally used to constrain the objective function according to the intrinsic property of the target [17]. This paper selects the total variational (TV) regularizer [18]. Two-step iterative shrinkage/thresholding (TwIST) is an effective algorithm to solve constrained optimization problems, which can realize reconstruction quickly and efficiently [19]. In this paper, TwIST is used to reconstruct the polarization spectrum data cube.

5 Experiment

5.1 Hardware Implementation

The experimental device includes (1) objective lens L1, (2) bandpass filter (BPF), (3) coded aperture (CA), (4) an F/8 relay lens L_2, (5) a double Amici prism (DAP), (6) a monochromatic pixelized polarized CMOS detector (P-detector). The cutoff range of BPF is 450 nm-650 nm. The CA includes 520 × 520 elements of random binary pattern with 13.8 μm× 13.8 μm in size. The central wavelength of the double Amici prism is 550 nm. The resolution of the pixelized polarized CMOS detector is 2448 × 2048, and the pixel size is 3.45 μm× 3.45 μm. Adjacent polarizers of 0°, 45°, 90° and 135° are placed on the array [20, 21] (Fig. 3).

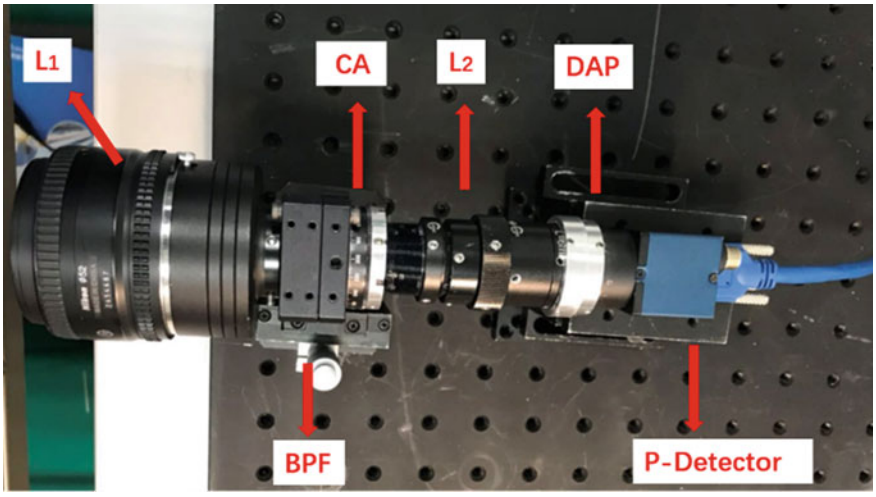

Fig. 3 Experimental prototype developed at laboratory

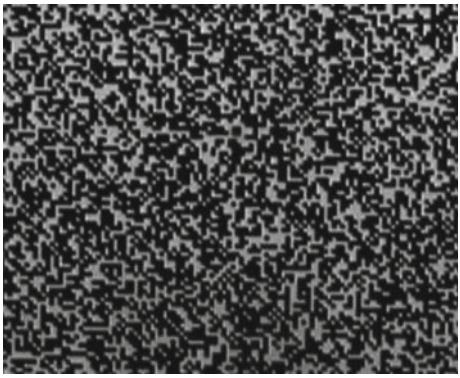

Fig. 4 Coded aperture image obtained at a wavelength of 614 nm

5.2 Calibration

A monochromator is used as the light source. The wavelength ranges in 450–650 nm, and the wavelength interval is 1 nm. The center wavelength is determined, and its position corresponds to the pixels on the detector. Twenty-five wavelengths are selected as the basis of reconstruction, and the coded aperture spectrum image of the corresponding wavelength is obtained. In order to eliminate dark current noise, 10 dark current noise images of each wavelength were acquired. The calibration images at different wavelengths are averaged in energy, and then the exposure time during the calibration process is equivalent to a constant [22–24] (Fig. 4).

5.3 Experiment Results

In Fig. 5, the scene consists of a blue book, a red racket, a color card and a checkerboard. The polarization angles are 0°, 45°, 90° and 135°. An image with no polarization angle was acquired.

Spectral and polarization information can be reconstructed by TwIST. Figure 6 shows the reconstructed results of four polarization angles (0°, 45°, 90° and 135°) ranging in 450–650 nm, including 25 bands, using a color display at the corresponding wavelength.

The Stokes parameters S_0, S_1, S_2, S_3 are calculated and displayed in 3D after correction [13], the x-axis and the y-axis represent the spatial domain, and the z-axis represents the spectral domain.

$$S = \begin{bmatrix} S_0 \\ S_1 \\ S_2 \\ S_3 \end{bmatrix} = \begin{cases} S_0 = I_0 + I_{90} \\ S_1 = I_0 - I_{90} \\ S_2 = I_{45} - I_{135} \\ S_3 = I_R - I_L \end{cases} \tag{9}$$

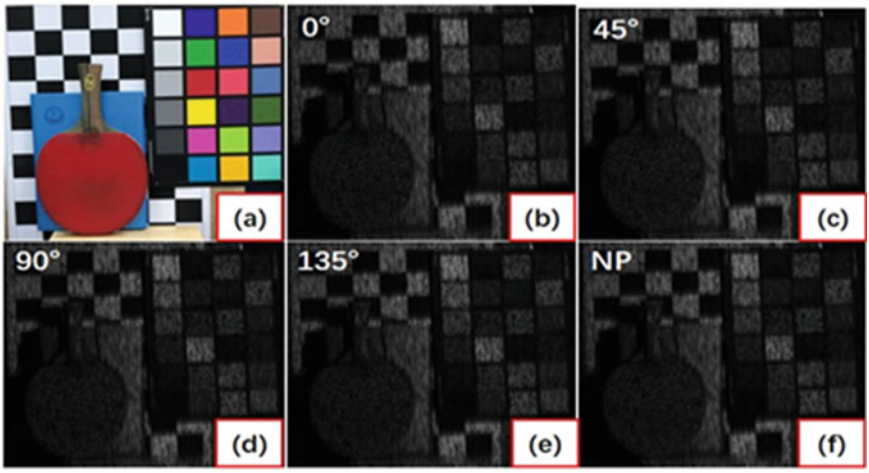

Fig. 5 Experimental scene and measured images. **a** The experimental scene, **b–e** different polarization components (0°, 45°, 90° and 135°), **f** no polarization image

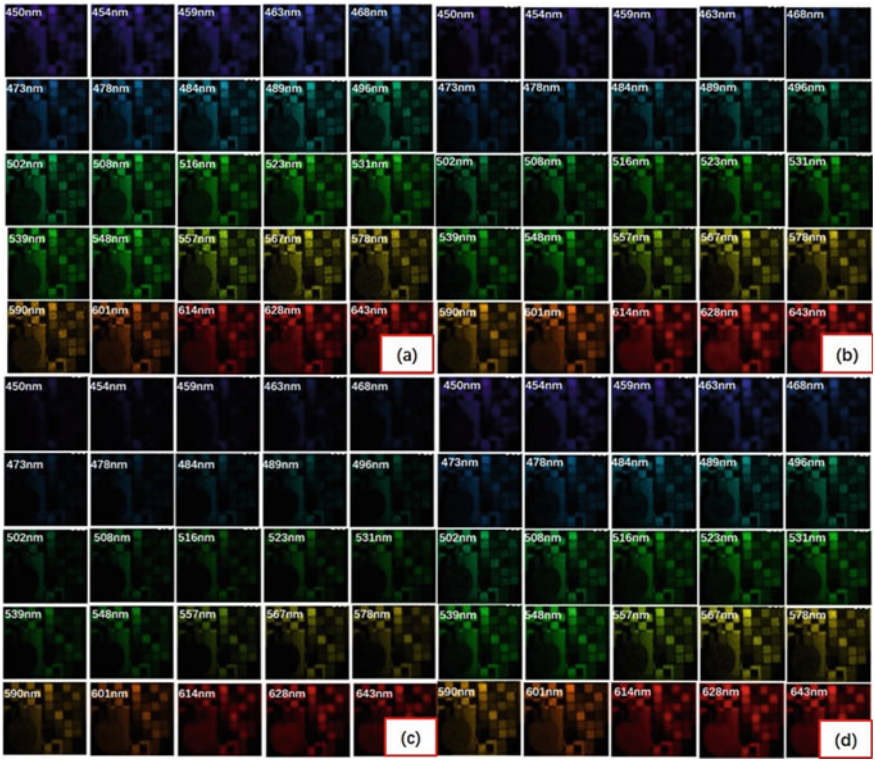

Fig. 6 Reconstructed results. **a–d** represent 0°, 45°, 90° and 135° polarization components

The circularly polarized Stokes parameter is assumes as [8]

$$S_3 = 0.1\left(S_0 - \sqrt{S_1^2 + S_2^2}\right) \tag{10}$$

Figure 7 indicates that S_1, S_2 and S_3 are significantly weaker than S_0, which can be explained by the properties of the Stokes parameters [25]. S_0 represents the total intensity of light, including the polarization component and the non-polarization component. S_1 is the difference between the horizontally polarized light and the vertically polarized light. S_2 is the difference between 45° and 135° polarized lights. Both S_1 and S_2 represent linearly polarized components. S_3 is the difference between the left and right circularly polarized lights and represents a circularly polarized light component. The main component of the light reflected by the natural scene is unpolarized light. The target to be measured is a natural scene, so it is mainly an unpolarized component [1].

Degree of linear polarization (DoLP) and angle of polarization (AoP) are defined as [1]

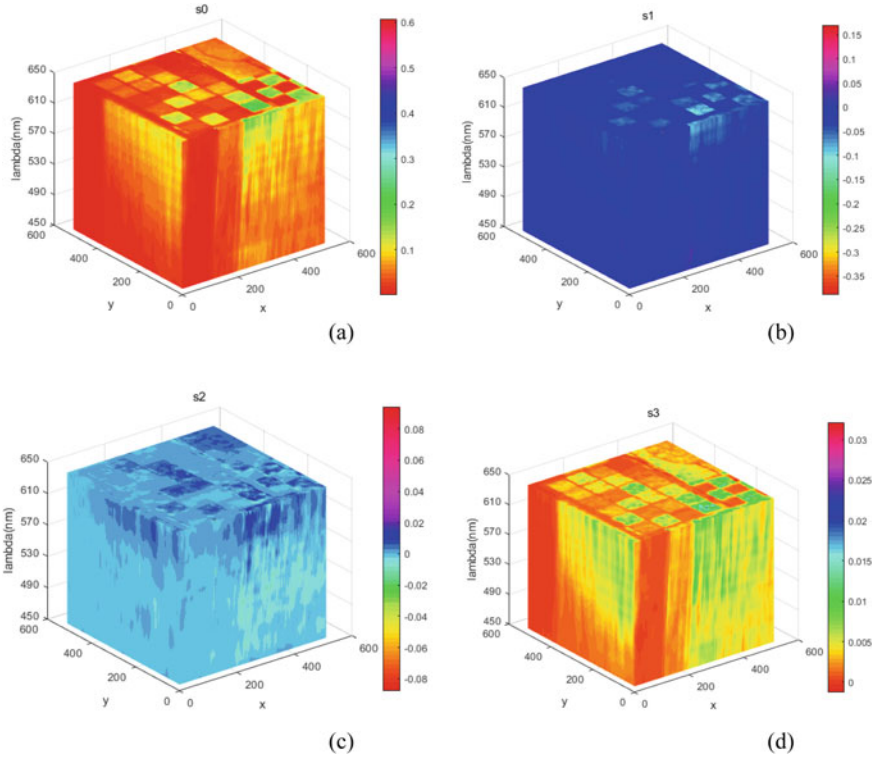

Fig. 7 Reconstructed results. **a–d** The 3D data cubes of S_0, S_1, S_2 and S_3

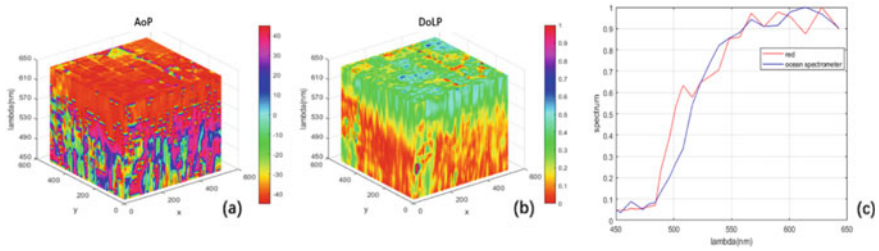

Fig. 8 **a**–**b** 3D image of AoP and DoLP, **c** reconstructed spectral curve of the red card and the blue curve is obtained by a spectrometer

$$\mathrm{DoLP} = \sqrt{S_1^2 + S_2^2}/S_0 \tag{11}$$

$$\mathrm{AoP} = \arctan(S_1/S_2)/2 \tag{12}$$

Figure 8a, b indicates that the edges of the checkerboard and the racket can be distinguished easily. The weaker area corresponds to a smaller AoP and a smaller DoLP. The area with much polarized characteristics is a larger AoP and medium DoLP. The results indicate that the spectral image with polarization information is easier to distinguish the edge of the object compared with the simple spectral imagery. (c) shows that the reconstructed spectra have good accuracy.

6 Conclusion

This paper proposes a new multidimensional polarization spectrum detection technology based on CASSI and a pixelized polarization detector. The system can simultaneously acquire spatial, spectral and polarization information. The CASSI performs the spatial coding modulation and the spectral dispersion aliasing compression sampling of the scene. The polarization information is acquired by the pixelized polarization detector. The polarization spectrum is reconstructed by TwIST. Compared with the existing polarization spectrum detection technology, the linear compression sampling model does not require Fourier transform and spatial filter. The technology improves the luminous flux and the noise sensitivity, and spectral resolution reduction and channel cross talk caused by traditional polarization spectrum acquisition technology got improved and eliminated. Acquisition of polarization spectrum with 25 bands' range in 450–650 nm using the technology is demonstrated. The feasibility has been successfully verified by the experiment.

References

1. Tyo JS, Goldstein DL, Chenault DB, Shaw JA (2006) Review of passive imaging polarimetry for remote sensing applications. Appl Opt 45:5453–5469
2. Oka K, Kato T (1999) Spectroscopic polarimetry with a channeled spectrum. Opt Lett 24:1475–1477
3. Kudenov MW, Hagen NA, Dereniak EL, Gerhart GR (2007) Fourier transform channeled spectropolarimetry in the mwir. Opt Express 15:12792–12805
4. Chan VC, Kudenov M, Liang C, Zhou P, Dereniak E (2014) Design and application of the snapshot hyperspectral imaging fourier transform (shift) spectropolarimeter for fluorescence imaging. Proc SPIE 8949:894–903
5. Mu T, Zhang C, Li Q, Wei Y, Chen Q, Jia C (2014) Snapshot full-stokes imaging spectropolarimetry based on division-of-aperture polarimetry and integral-field spectroscopy. Proc SPIE 9298:92980D
6. Locke AM, Salyer D, Sabatke DS, Dereniak EL (2003) Design of a SWIR computed tomographic imaging channeled spectropolarimeter. Proc. SPIE 5158:507136
7. Dereniak EL, Craven JM, Kudenov MW (2009) False signature reduction in infrared channeled spectropolarimetry. Proc SPIE 7419:7419
8. Yiren W, Fu C, Wu D, Xie Y (2019) Channeled compressive imaging spectropolarimeter. Opt Exp 27(3l4)
9. Candès EJ, Wakin MB (2008) An introduction to compressive sampling. IEEE Signal Process Mag 25:21–30
10. Wagadarikar A, John R, Willett R, Brady D (2008) Single disperser design for coded aperture snapshot spectral imaging. Appl Opt 47:B44–B51
11. Arce GR, Brady DJ, Carin L, Arguello H, Kittle DS (2014) Compressive coded aperture spectral imaging: an introduction. IEEE Signal Process Mag 31(1):105–115
12. Tan J, Ma Y, Rueda H, Baron D, Arce GR (2016) Compressive hyperspectral imaging via approximate message passing. IEEE J Sel Top Signal Process 10:389–401
13. Chipman RA (2009) Handbook of optics. McGraw-Hill
14. Kalibjian R (2004) Stokes polarization vector and Mueller matrix for a corner-cube reflector. Opt Commun 240:39–68
15. Arce GR, Brady DJ, Carin L, Arguello H, Kittle DS (2014) Compressive coded aperture spectral imaging: an introduction. IEEE Signal Process Mag 31:105–115
16. Zibulevsky M, Elad M (2010) L1-l2 optimization in signal and image processing. IEEE Signal Process Mag 27(3):76–88
17. Daubechies I, DeVore R, Fornasier M, Güntürk CS (2010) Iteratively reweighted least squares minimization for sparse recovery. Commun Pure Appl Math 63(1):1–38
18. Tsai T-H, Brady DJ (2013) Coded aperture snapshot spectral polarization imaging. Appl Opt 52:2153–2161
19. Bioucas-Dias JM, Figueiredo MA (2007) A new twist: two-step iterative shrinkage/thresholding algorithms for image restoration. IEEE Trans Image Process 16:2992–3004
20. Zhao X, Boussaid F, Bermak A, Chigrinov VG (2009) Thin photopatterned micropolarizer array for CMOS image sensors. IEEE Photon Technol Lett 21:805–807
21. Tokuda T, Sato S, Yamada H, Sasagawa K, Ohta J (2009) Polarisation-analysing CMOS photosensor with monolithically embedded wire grid polarizer. Electron Lett 45:228–230
22. Wagadarikar Ashwin A, Pitsianis Nikos P, Sun Xiaobai, Brady David J (2008) Spectral image estimation for coded aperture snapshot spectral imagers. SPIE 7076:707602
23. Ma X, Wang Z, Li Y, Arce GR, Dong L, Garcia-Frias J (2018) Fast optical proximity correction method based on nonlinear compressive sensing. Opt Express 26:14479–14498
24. Powell SB, Gruev V (2013) Calibration methods for division-of-focalplane polarimeters. Opt Express 21:21039–21055
25. Stokes GG (1852) On the composition and resolution of streams of polarized light from different sources. Trans Cambridge Philos Soc 9:399–416